Finite Element Analysis of Reinforced Concrete Structures

Proceedings of the Seminar sponsored
by the Japan Society for the Promotion of Science
and the U.S. National Science Foundation

Tokyo, Japan
May 21-24, 1985

Approved for publication by the
Structural Division of the
American Society of Civil Engineers

Edited by Christian Meyer, Columbia University, New York
and
Hajime Okamura, University of Tokyo

Published by the
American Society of Civil Engineers
345 East 47th Street
New York, New York 10017-2398

FRACTURE MECHANICS AND STRAIN-SOFTENING OF CONCRETE

Zdeněk P. Bažant,[1] F.ASCE

ABSTRACT: Finite element analysis of failure of certain types of concrete structures requires modeling of distributed cracking. Propagation of failure zones with distributed cracking must be treated from the viewpoint of fracture mechanics if the calculation should be objective and properly converge as the mesh is refined. After a brief review of the crack band model, it is shown that this model is applicable to both localized and nonlocalized cracking, while the strain-softening fracture models based on line cracks are applicable only to localized cracking. The article subsequently expounds a novel approach to strain-softening—a nonlocal formulation in which stress at a point depends on the entire strain field from a neighborhood of the point. Application of the theory is demonstrated by finite element analysis of waves in strain-softening materials. Furthermore, the formulation of strain-softening constitutive relations on the basis of the microplane model is briefly outlined, and the size effect is discussed. Finally, the structural size effect is analyzed and a generalized form of the size effect law is presented.

INTRODUCTION

Heterogeneous brittle materials such as concretes or rocks fail by *progressive fracturing distributed over a finite-size zone within the* material. In the continuum approximation, this zone is characterized by strain-softening, i.e., a stress-strain relation in which the maximum principal stress decreases at increasing strain. The purpose of the present article is to present an overview of some recent results obtained at Northwestern University in the use of strain-softening material models for the description of fracture propagation in concrete structures.

CRACK BAND MODEL

Due to the distributed nature of microcracking, as well as the fact that the path of a final crack is generally not smooth but highly tortuous, it is not unrealistic to model cracking by means of stress-strain relations characterized by strain-softening in which the major principal tensile stress is gradually reduced to zero at increasing strain (Fig. 1). This approach is particularly convenient for finite element analysis, since it necessitates merely an adjustment in the incremental stiffness matrix of the finite element.

In the form of sudden cracking, this approach was introduced in 1967 by Rashid (34,49). For strain-softening analysis of fracture this ap-

[1]Professor of Civil Engineering and Director, Center for Concrete and Geomaterials, Northwestern University, Evanston, Illinois 60201, USA.

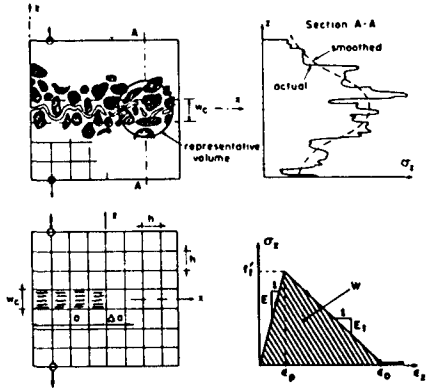

Figure 1. Fracture in a heterogeneous aggregate material, statistical scatter of stress, crack band model, and strain-softening stress-strain diagram

proach was extended in Refs. 5, 24, in which the strain-softening triaxial stress-strain relation was formulated as:

$$\underset{\sim}{\varepsilon} = \underset{\sim}{D}\underset{\sim}{\sigma} + \underset{\sim}{\xi}. \tag{1}$$

Here $\underset{\sim}{\varepsilon}$ and $\underset{\sim}{\sigma}$ are the column matrices of the components of strain and stress, $\underset{\sim}{D}$ is the 6×6 matrix of variable secant elastic compliances and $\underset{\sim}{\xi} = (\xi_{11},\xi_{22},\xi_{33},0,0,0)^T$, where superscript T denotes a transpose and the numerical subscripts refer to cartesian coordinates x_i ($i = 1,2,3$); $\underset{\sim}{\xi}$ is the column matrix of additional smeared-out strains due to cracking. The normal stresses are assumed to be uniquely related to their associated cracking strains (Fig. 1), i.e.,

$$\sigma_{11} = C(\xi_{11})\xi_{11}, \quad \sigma_{22} = C(\xi_{22})\xi_{22}, \quad \sigma_{33} = C(\xi_{33})\xi_{33} \tag{2}$$

in which C is the secant modulus for cracking strain. C reduces to zero at very large cracking strain and may be calibrated from direct tensile test data (33,35,44,45,50,51). Different algebraic relations are used for unloading. In the simplest form of the model it is assumed that cracking can occur only in three mutually orthogonal directions which are known in advance and do not rotate against the material once the cracking starts. For details of the procedure, see Ref. 24. Cracking in all directions can be described by the microplane model (see Eq. 29).

In the classical formulation of finite element analysis of concrete structures, as employed in the current large computer programs, a strain-softening stress-strain relation, usually one that exhibits a sudden stress drop, is used indiscriminately for an arbitrarily chosen finite element size. It has been demonstrated, however, that this approach is inconsistent, unobjective with regard to the analyst's choice of the element size. It can yield greatly different results for different mesh sizes (6,9,16-18). For failures of the brittle type, the load causing further fracture extension converges to zero as the mesh size tends to zero and so does the total energy consumed by failure of the structure. These are physically unrealistic results (4,16,20).

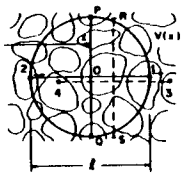

Figure 2. Characteristic volume of a heterogeneous material

It has been shown that these incorrect features can be eliminated by using an energy criterion rather than the stress-strain relation as the primary condition for the extension of the cracked band of finite elements. Considering a crack band of a single-element width, consisting of finite elements with a uniform strain distribution across the band, the fracture energy, i.e., the energy consumed per unit extension of the crack band (and per unit thickness), may be expressed as

$$G_f = w_c \int \sigma_{33} d\varepsilon_{33} = \frac{w_c}{2} f_t'^2 \left(\frac{1}{E_0} - \frac{1}{E_t}\right) \tag{3}$$

in which w_c is the width of the crack band front, which must be considered as a material property (4), σ_{33} is the normal stress across the central plane of the crack band, f_t' is the direct tensile strength of the material, E_0 is the initial elastic Young's modulus, and E_t is the mean downward slope of the strain-softening segment of the stress-strain diagram, which is negative; w_c may be approximately considered as $3d_a$ where d_a = maximum aggregate size.

It was shown (24) that the crack-band finite element model yields results which agree with all essential experimental evidence from fracture tests, both the maximum load data and the R-curves (9,55). However if the cracking at the failure front tends to localize into a single-element width, a behavior which fracture specimens are designed to ex-

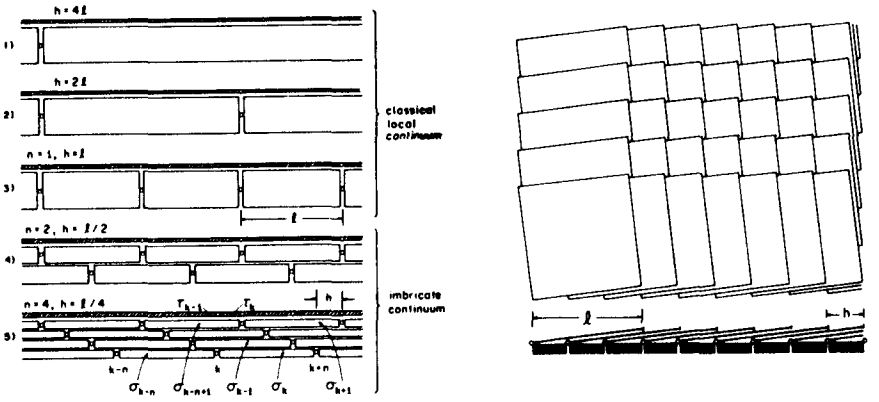

Figure 3. Illustration of mesh refinement for a one-dimensional imbricate continuum (left) and of element arrangement for a two-dimensional imbricate continuum (right) (the elements are slightly rotated for the purpose of illustration)

hibit, then the use of the correct element size $h = w_c$ is essential. For large structures, such elements are impracticably small, and a larger element size needs to be used. It was shown (16-18,24) that this leads to consistent results if the value of fracture energy G_f is preserved. This can be achieved by first adjusting the value of E_t, and if $E_t \to -\infty$ (vertical drop), by adjusting also f_t' while always satisfying Eq. 3, in which w_c is replaced by h. So, one must use some equivalent strain-softening slope and some equivalent tensile strength, depending on the element size, if consistent results should be achieved.

On the other hand, one may also imagine the width of the crack band to be reduced to zero, and if the strain-softening slope E_t is adjusted so as to keep the correct value of G_f, the model in the limit becomes equivalent to the use of the stress-displacement relation on the centerline of fracture. This limiting case of the crack band model coincides with the model of Hillerborg et al. (36,44).

The adjustment of constitutive properties in order to achieve consistent results for different mesh sizes is, however, disconcerting from the fundamental, mathematical viewpoint. It appears as if the finite element model was approximating a continuum that is actually not defined. Obviously, in the crack band model we cannot say we are approximating the solution for a classical, local continuum because for such a continuum the crack band in fact can localize into a layer of zero thickness, while an adjustment of material properties is not permitted.

The source of the difficulty appears to be (7,19) the assumption that we deal with a local continuum, in which the stress at a certain point is a function of the strain at the same point. We now focus attention on the development of a new type of continuum for which the aforementioned mathematical difficulties do not arise. At the same time we gain with this new type of continuum a means to resolve in detail the distributions of the averaged stress and strain throughout the cracking zone.

NONLOCAL CONTINUUM APPROACH

From the works of Kröner and others (39-43), it is known that in a statistically heterogeneous medium which is not in a macroscopically homogeneous state of strain, the averaged (smoothed, homogenized) stress at a certain point depends not only on the gradient of the averaged displacement at that same point (local properties), but also on the averaged displacements within a certain characteristic finite neighborhood of that point. The properties of such a medium cannot, therefore, be said to be local, and the medium is called nonlocal. The nonlocal displacement gradient may be defined by the relation

$$D_i u_j(\underset{\sim}{x}) = \frac{1}{V}\int_{V(\underset{\sim}{x})} \frac{\partial u_j(\underset{\sim}{x}')}{\partial x_i}\, dV' = \frac{1}{V}\int_{S(\underset{\sim}{x})} u_j(\underset{\sim}{x}')n_i(\underset{\sim}{x}')dS' \qquad (4)$$

in which u_j are the cartesian displacement components (j = 1,2,3), $\underset{\sim}{x}$ is the coordinate vector characterized by cartesian coordinates x_i, $V(\underset{\sim}{x})$ is the characteristic volume of the material (Fig. 2) centered at point $\underset{\sim}{x}$, $S(x)$ is the surface of this volume, $n_i(\underset{\sim}{x}')$ is the unit normal of this surface at point $\underset{\sim}{x}'$, and D_i is the gradient averaging operator. The surface integral in Eq. 4 follows from the volume integral by application of the Gauss integral theorem. More generally, a weighting function can be introduced in Eq. 4. Using the gradient averaging operator, the mean strains may be defined as

$$\bar{\varepsilon}_{ij} = \tfrac{1}{2}(D_i u_j + D_j u_i). \qquad (5)$$

In previous works dealing with nonlocal continua it has been generally assumed that the continuum equation of motion may be written as

$$\frac{\partial}{\partial x_j}\bar{C}_{ijkm}(\bar{\underset{\sim}{\varepsilon}})\, D_m u_k = \rho\ddot{u}_i \qquad (6)$$

in which C_{ijkm} are the secant elastic moduli which, in general, depend on the mean strain, ρ is the mass density, and superior dots refer to time derivatives. It is found, however, that Eq. 6 is incapable of describing a strain-softening continuum. It always leads to unstable response as soon as strain-softening begins. The difficulty has been traced to the asymmetry of these equations which consists in the combination of partial derivatives $\partial/\partial x_j$ with the gradient averaging operator D_m. This nonsymmetry gives rise to nonsymmetric finite element matrices even if C_{ijkm} are constant, i.e., if the medium is elastic. Such a nonsymmetry is certainly an objectional property.

For this reason, a systematic derivation of the continuum equation of motion on the basis of Eq. 4 was attempted, using the calculus of variations. It was found (19,7)that the proper form of the continuum equation of motion is

$$(1-\gamma)D_j\bar{C}_{ijkm}(\bar{\underset{\sim}{\varepsilon}})D_m u_k + \gamma\frac{\partial}{\partial x_j}C_{ijkm}(\underset{\sim}{\varepsilon})\frac{\partial}{\partial x_m}u_k = \rho\ddot{u}_i \qquad (7)$$

in which γ is an empirical coefficient between 0 and 1, and C_{ijkm} are the local secant moduli. In contrast to Eq. 6, each term of the last equation has a symmetric structure, and consequently, discretization by finite elements leads to symmetric stiffness matrices if the elastic moduli $\bar{C}_{ijkm}$ and C_{ijkm} are symmetric. To prevent instabilities which involve periodic zero-energy deformation modes, it is necessary that $\gamma > 0$. However, if γ is close to 0 there is excessive noise in the numerical solution, and to avoid it, γ should not be chosen less than about 0.1, as experience shows (19).

Eq. 7 can also be written in the form

$$(1-\gamma)D_j\sigma_{ij} + \gamma\,\tau_{ij,j} = \rho\,\ddot{u}_i \qquad (8)$$

in which the subscript following a comma denotes a partial derivative and

$$\sigma_{ij} = \bar{C}_{ijkm}(\bar{\underset{\sim}{\varepsilon}})\varepsilon_{km} = \bar{C}_{ijkm}(\bar{\underset{\sim}{\varepsilon}})D_m u_k \qquad (9)$$

$$\tau_{ij} = C_{ijkm}\,\varepsilon_{km} = C_{ijkm}\,u_{k,m}. \qquad (10)$$

τ_{ij} are the usual, local stresses, and σ_{ij} are the stresses characterizing the stress state in the entire representative volume of the material, called the broad-range stresses (7,19).

When the continuum defined by Eq. 7 or 8 is discretized by finite elements the size of which is smaller than the size ℓ of the representative volume, one obtains a system of overlapping (or imbricated) finite elements visualized in Fig. 3. Therefore, the present type of nonlocal continuum has been called imbricate. The finite elements keep a constant

size ℓ as the mesh is refined, and the number of finite elements crossing a given point is inversely proportional to the mesh size, while the cross section of these elements diminishes so that all imbricated elements have the same total cross section for any mesh size. It can also be shown that the limiting case of the finite difference equations describing such an imbricated system of finite elements is the differential equation in Eq. 7 or 8 (7,19). If the finite element size h is larger than the characteristic length ℓ, then the finite element model of the imbricate continuum becomes identical to that for the classical local continuum.

To assure convergence and stability, the local stress-strain relations (Eq. 10) may not exhibit strain-softening, or else unstable response and spurious sensitivity to mesh size, along with incorrect convergence, may be obtained. The strain-softening properties must be described solely by the broad-range stress-strain relation in Eq. 9.

EXAMPLES: WAVES IN STRAIN-SOFTENING MATERIALS

To demonstrate that the concept of imbricate nonlocal continuum yields convergent finite element solutions for problems with a finite-size strain-softening zone, we will now describe two examples of one-dimensional waves. As the first example, Fig. 4 reproduces some of the results of explicit dynamic finite element calculations from Ref. 19, in which wave propagation in a strain-softening bar of length ℓ was analyzed. The characteristic length ℓ for nonlocal solution is assumed to be 1/5 of bar length L. Both ends of the bar are subjected to a constant outward velocity v_0 beginning at time $t = 0$. This loading produces step waves of strain propagating inward. When these waves meet at midlength, the strain suddenly increases and strain-softening ensues.

If this problem is analyzed with the usual finite element method for local continuum, it is found that strain-softening always localizes into a single finite element. Thus, the width of the strain-softening zone reduces to zero as the element mesh is refined. Since the energy dissipation per unit volume equals the area under the stress-strain diagram, which is finite, the energy W consumed by failure decreases with decreasing mesh size and approaches zero as the mesh size tends to zero (Fig. 5), which is unrealistic from the physical point of view. Moreover, the finite element model of local continuum exhibits a discontinuous dependence of response on the prescribed end velocities as well as on the slope E_t of the strain-softening branch (12). The solution, however, converges to a unique exact solution (12) and the convergence is quadratic.

By contrast, for the present imbricate continuum, the solution of wave propagation in the strain-softening bar exhibits correct convergence, with a strain-softening zone of a finite size in the limit (Fig. 4, right column). Also, the energy consumed by failure in the bar converges to a finite value, as shown in Fig. 5.

As another example, we now briefly describe the solution for an implosive (converging) spherical wave, a problem which was proposed by T. Belytschko and was originally solved in full detail in Ref. 28. Although this problem is also one-dimensional it involves three-dimensional stress and strain states. Like for the bar problem, strain-softening is produced inside the body but there is an important difference — waves

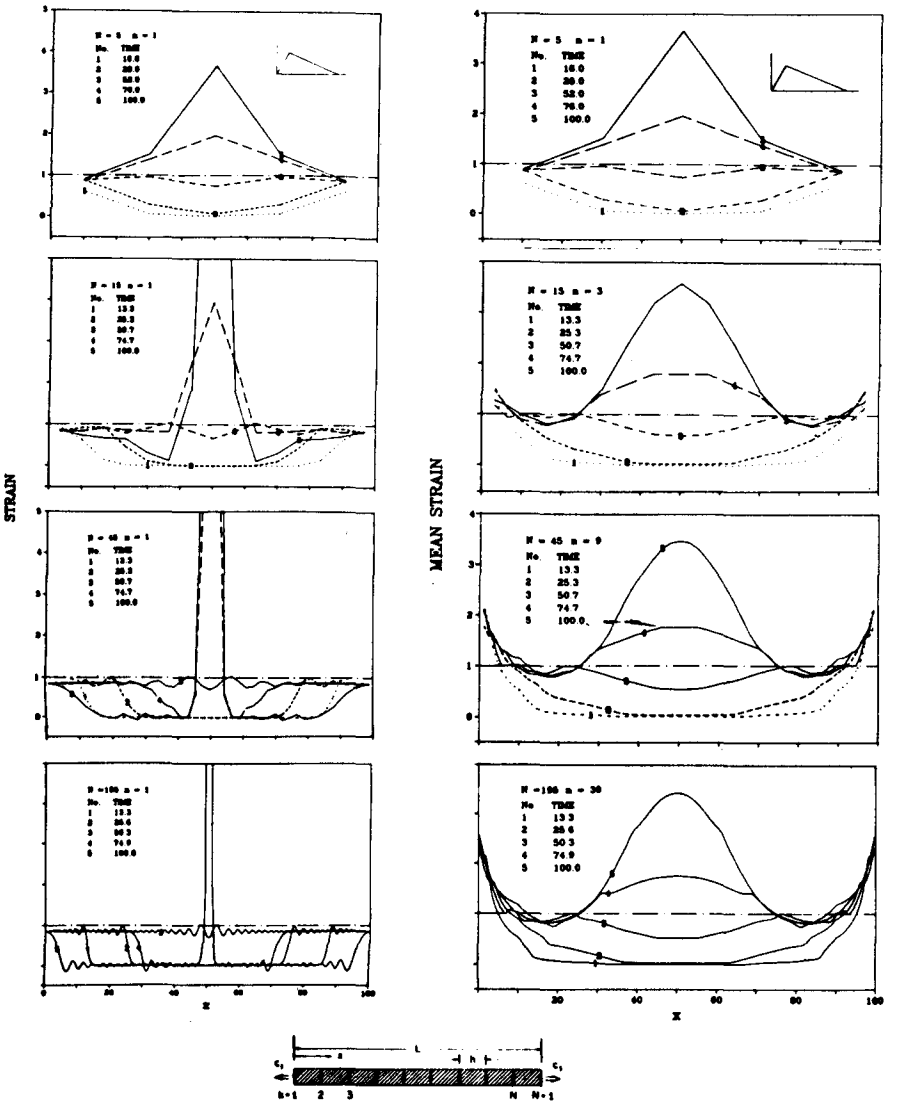

Figure 4. Numerical results of Bažant, Chang and Belytschko (19) for wave propagation in a strain-softening bar, obtained with different numbers N of identical elements (left column - local continuum, right column - imbricate nonlocal continuum)

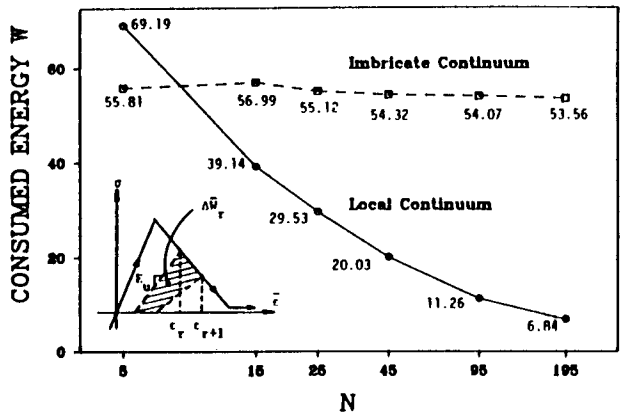

Figure 5. Energy consumed by failure caused by wave propagation in a one-dimensional bar

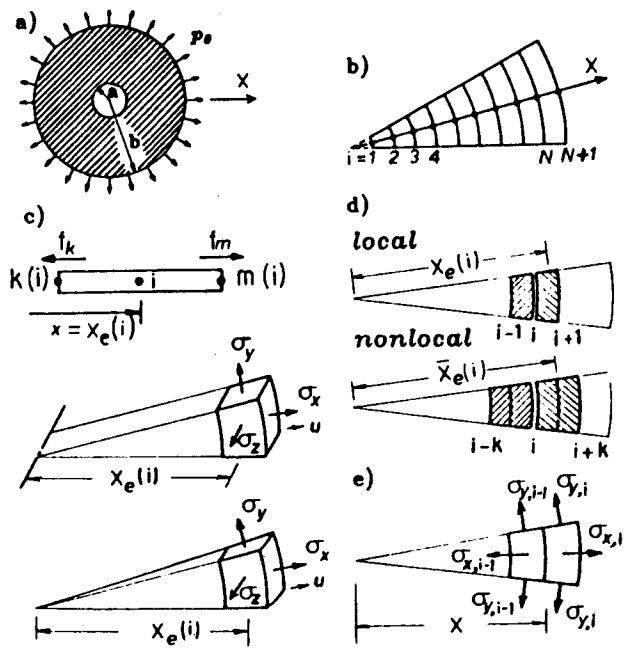

Figure 6. Spherical waves and finite elements in spherical coordinates

can pass through the points of strain-softening even if a local continuum is assumed.

We consider a wave generated by a sudden application of a constant uniform pressure p at the exterior surface of a hollow sphere. The pressure is a Heaviside step function of time, i.e., the boundary condition at $x = b$ (Fig. 6a) is $\sigma_x = p_0 H(t)$, and the interior surface is load-free, i.e., $\sigma_x = 0$ at $x = a$ (a,b = internal and external surface radii, x = radial coordinate). Initially, at $t = 0$, the body is at rest. The elastic solution, as is well known (1), consists of a wave with a step front of strain whose magnitude is growing as the wave front propagates toward the center. Therefore, at a certain time t_1 (and at $x = x_1$) the strain at the wavefront reaches the elastic limit, and if the material has strain-softening properties, strain-softening is thus produced in the interior of the solid by a one-directional wave, while for uniaxial waves (planar wavefront) strain-softening can be produced in the interior only if waves of opposite directions meet.

The governing differential equations in spherical coordinates are:

$$\varepsilon_x = u_{,x}, \quad \varepsilon_y = \frac{u}{x}, \quad \varepsilon_z = \varepsilon_y \tag{11}$$

$$\varepsilon = \varepsilon_x + 2\varepsilon_y, \quad e_x = \frac{2}{3}(\varepsilon_x - \varepsilon_y), \quad e_y = \frac{1}{3}(\varepsilon_y - \varepsilon_x) \tag{12}$$

$\bar{\varepsilon}_x, \bar{\varepsilon}_y, \bar{\varepsilon}, \bar{e}_x, \bar{e}_y$ = the means of $\varepsilon_x, \varepsilon_y, \varepsilon, e_x, e_y$ analogous to Eqs. 11 and 16 (13)

$$\sigma_{x,t} = \bar{K}\,\bar{\varepsilon}_{,t} + 2\bar{G}\,\bar{e}_{x,t}, \quad \sigma_{y,t} = \bar{K}\,\bar{\varepsilon}_{,t} + 2\bar{G}\,\bar{e}_{y,t} \tag{14}$$

$$\tau_{x,t} = K\,\varepsilon_{,t} + 2G\,e_{x,t}, \quad \tau_{y,t} = K\,\varepsilon_{,t} + 2G\,e_{y,t} \tag{15}$$

$$\bar{\sigma}_x(x) = \int_{x-\ell/2}^{x+\ell/2} \sigma_x(x+s)w(s)ds, \quad \bar{\sigma}_y(x) = \int_{x-\ell/2}^{x+\ell/2} \sigma_y(x+s)w(s)ds \tag{16}$$

$$S_x = (1-\gamma)\bar{\sigma}_x + \gamma\tau_x, \quad S_y = (1-\gamma)\bar{\sigma}_y + \gamma\tau_y \tag{17}$$

$$S_{x,x} + \frac{2}{x}(S_x - S_y) = \rho u_{,tt}\,. \tag{18}$$

Here ℓ = characteristic length of material = size of representative volume, u = radial displacement, x = radial coordinate (Fig. 6a); $\varepsilon_x, \varepsilon_y$ = radial and circumferential normal strains (local); ε, e_x, e_y = volumetric strain (= volume change) and deviatoric strains (local), τ_x, τ_y = local radial and circumferential normal strains; σ_x, σ_y = broad-range radial and circumferential normal stress; S_x, S_y = total radial and circumferential normal stresses, K, G, $\bar{K}$, $\bar{G}$ = local and broad-range (nonlocal) bulk and shear moduli. In Eq. 18, isotropy of the material is assumed. The shear moduli G and $\bar{G}$ are assumed to be constant, while K and $\bar{K}$ depend on ε and $\bar{\varepsilon}$, respectively; $K > 0$ but $\bar{K}$ may become negative, which represents strain-softening. Eq. 18 represents the differential equations of motion of the usual form (1).

For elastic spherical wave, the present problem has a closed-form solution:

$$u = -\frac{b^3 p_0}{4Gr^2}\left\{1 - e^{\xi\tau}\left[\frac{\xi}{\omega}\left(\frac{2r}{b} - 1\right)\sin\omega\tau + \cos\omega\tau\right]\right\} \quad \text{for } \tau > 0 \tag{19}$$

as may be checked by substituting in Eqs. 11-18 with $\gamma = 1$, and $K =$ constant; and

$$\tau = t - (b-r)/c_1, \quad \xi = 2c_2^2/(bc_1), \quad \omega = \xi[(c_1/c_2)^2 - 1]^{\frac{1}{2}},$$
$$c_1 = [3K(1-\nu)/(1+\nu)\rho]^{\frac{1}{2}}, \quad c_2 = (G/\rho)^{\frac{1}{2}}, \quad \nu = (3K-2G)/(6K+2G). \tag{20}$$

For the purpose of numerical solution, a one-dimensional mesh with constant step h is used (Fig. 6b). All finite elements are two-node elements with a linear distribution of displacement u, integrated with a single numerical integration point at the element center. This is true of both the local elements of length h and the imbricate elements of length $\ell = nh$. Mass is lumped in the nodes. The radial nodal forces are referred to a radial conical segment of the sphere such that its cross section area at a unit distance from the center of coordinates is 1. The computational algorithm is similar to the usual explicit algorithm and is as follows:

1. Read a, b, ℓ, n, Δt (time step), N_e, $\bar{N}_e$, N_k, N_t (numbers of all local and imbricate elements, of all modes and of time steps), γ, and p_0. Generate arrays $\hat{k}(i)$, $\hat{m}(i)$, $\ell_e(i)$, $x_e(i)$, $\bar{k}(i)$, $\bar{m}(i)$, $\bar{\ell}_e(i)$, $\bar{x}_e(i)$ giving the number of the left and right nodes of the i^{th} local or imbricate element, its length, and its coordinate at the center of element. Also generate externally applied nodal forces $f^{ext}_{k,r}$. Initialize as zero the values (for $r = 1$) of $v_{k,r}$, $m_{k,r}$, $\tau_{xk,r}$, $\tau_{yk,r}$, $\sigma_{yk,r}$, max ε_k, max $\bar{\varepsilon}_k$, $\tau_{\max \varepsilon,k}$, $\sigma_{\max \varepsilon,k}$, for all $k = 1,\ldots,N_e$ (local elements) and $k = 1,\ldots,\bar{N}_e$ (imbricate elements).

2. DO 8, $r = 2,\ldots,N_t$.

3. Initialize nodal forces $F_k = 0$, $f_k = 0$ (for all nodes, $k = 1,\ldots,N_k$).

4. DO 5, $i = 1,\ldots,N_e$ (local elements).

5. Set $k = k(i)$, $m = m(i)$, $x = x_e(i)$, and evaluate $\Delta\varepsilon_{xi,r} = (v_{m,r} - v_{k,r})\Delta t/h$, $\varepsilon_{xi,r} = \varepsilon_{xi,r-1} + \Delta\varepsilon_{xi,r}$, $\Delta\varepsilon_{yi,r} = (v_{m,r} + v_{k,r})\Delta t/2x$, $\varepsilon_{yi,r} = \varepsilon_{yi,r-1} + \Delta\varepsilon_{yi,r}$, and $\Delta\varepsilon_{i,r} = \Delta\varepsilon_{xi,r} + 2\Delta\varepsilon_{yi,r}$. Then call a subroutine which determines the incremental tangential moduli $K_{i,r}$, $G_{i,r}$ for the local elements from their strains $\varepsilon_{xi,r}$, $\varepsilon_{yi,r}$, $\varepsilon_{i,r}$ and also decides whether virgin loading, unloading or reloading applies. Then calculate $\Delta\tau_{xi,r} = K_{i,r}\Delta\varepsilon_{i,r} + 2G_{i,r}e_{xi,r}$, $\Delta\tau_{yi,r} = K_{i,r}\Delta\varepsilon_{i,r} + 2G_{i,r}e_{yi,r}$, $\tau_{xi,r-1} + \Delta\tau_{xi,r}$, $\tau_{yi,r} = \tau_{yi,r-1} + \Delta\tau_{yi,r}$. Then calculate all the local nodal forces at element nodes k and m (Fig. 6c);

$$\Delta f_k = -\gamma[\tau_{xi,r}x^2 - \tau_{yi,r}(x - \tfrac{h}{2})h], \quad \Delta f_m = \gamma[\tau_{xi,r}x^2 + \tau_{yi,r}(x + \tfrac{h}{2})h]. \tag{21}$$

These forces are accumulated at each node, $f_k \leftarrow f_k + \Delta f_k$, $f_m \leftarrow f_m + \Delta f_m$.

6. DO 7, $i = 1,\ldots,\bar{N}_e$ (imbricate elements).

7. Set $k = \bar{k}(i)$, $m = \bar{m}(i)$, $\ell = \bar{\ell}_e(i)$, $x = \bar{x}_e(i)$ and evaluate $\Delta\bar{\varepsilon}_{xi,r} = (v_{m,r} - v_{k,r})\Delta t/\ell$, $\bar{\varepsilon}_{xi,r} = \bar{\varepsilon}_{xi,r-1} + \Delta\bar{\varepsilon}_{xi,r}$, $\Delta\bar{\varepsilon}_{yi,r} = (v_{m,r} + v_{k,r})\Delta t/2x$, $\bar{\varepsilon}_{yi,r} = \bar{\varepsilon}_{yi,r-1} + \Delta\bar{\varepsilon}_{yi,r}$, and $\Delta\bar{\varepsilon}_{i,r} = \Delta\bar{\varepsilon}_{xi,r} + 2\Delta\bar{\varepsilon}_{y,r}$. Then call a subroutine which determines the incremental (tangential) moduli $\bar{K}_{i,r}$, $\bar{G}_{i,r}$ for the imbricate elements from their mean strains $\bar{\varepsilon}_{xi,r}$, $\bar{\varepsilon}_{yi,r}$, $\bar{\varepsilon}_{i,r}$

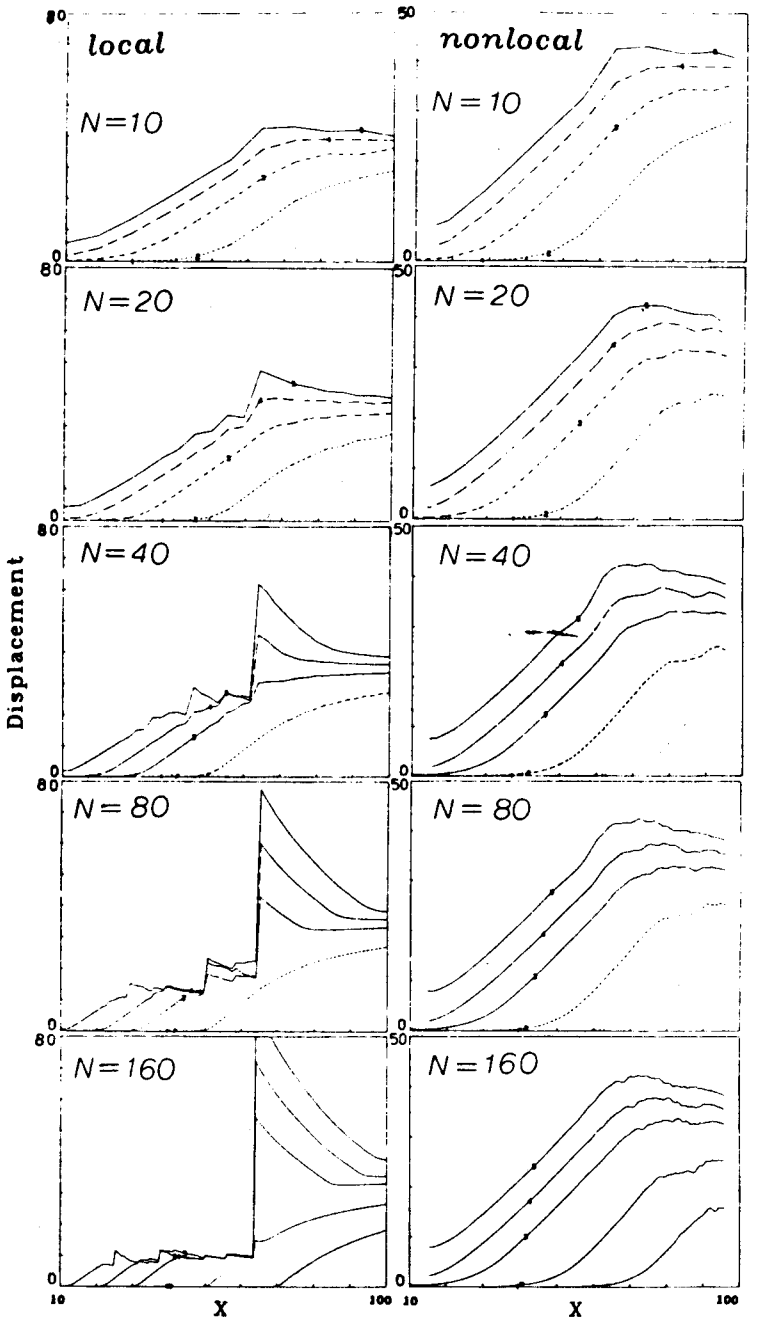

Figure 7. Radial displacement profiles at various times obtained for various finite element subdivisions (N = number of elements)

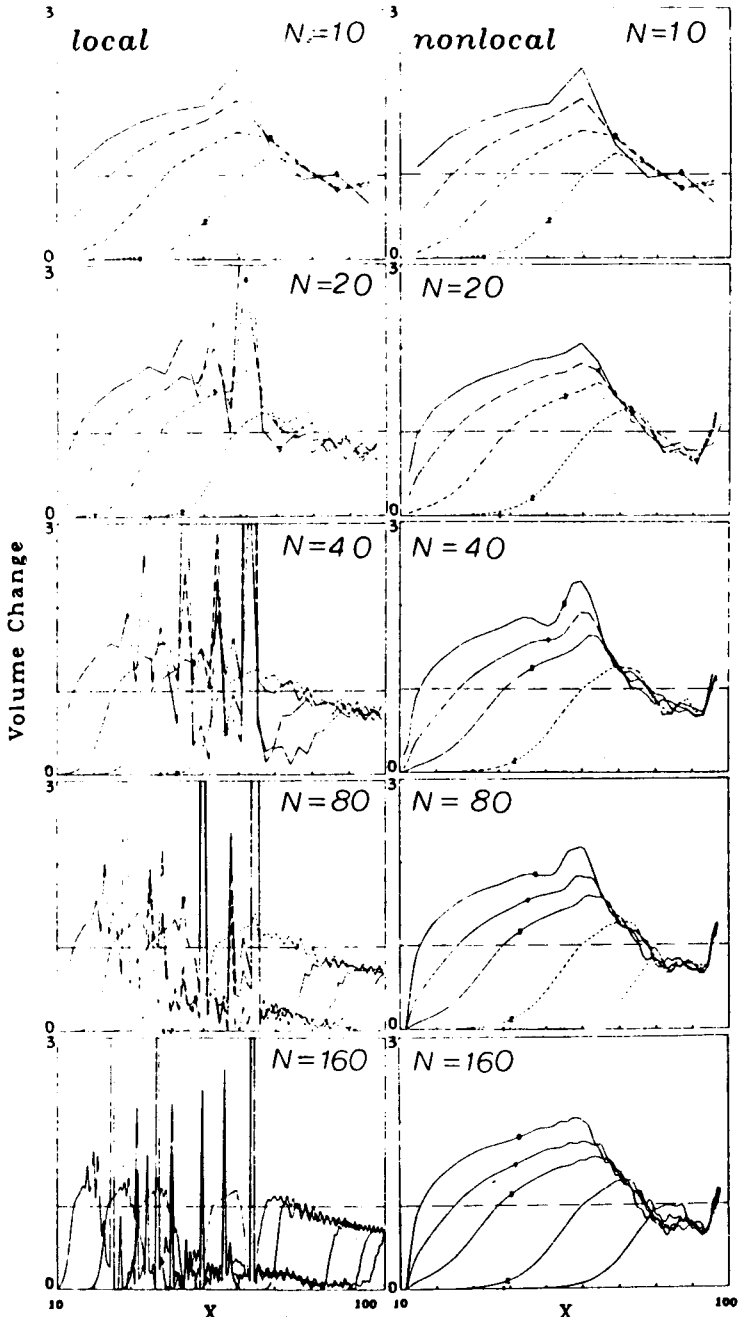

Figure 8. Volumetric strain profiles at various times obtained for various finite element subdivisions (N = number of elements)

and also decides whether virgin loading, unloading or reloading applies. Then calculate $\Delta\sigma_{xi,r} = \bar{K}_{i,r}\Delta\varepsilon_{i,r} + 2\bar{G}_{i,r}e_{xi,r}$, $\Delta\sigma_{yi,r} = \bar{K}_{i,r}\Delta\varepsilon_{i,r} + 2\bar{G}_{i,r}e_{yi,r}$, $\sigma_{xi,r} = \sigma_{xi,r-1} + \Delta\sigma_{xi,r}$, $\sigma_{yi,r} = \sigma_{yi,r-1} + \Delta\sigma_{yi,r}$. Further calculate all the nonlocal nodal forces at element nodes k and m (Fig. 6d):

$$\Delta F_k = -\frac{1-\gamma}{n}\left[\sigma_{xi,r}x^2 - \sigma_{yi,r}(x-\frac{h}{2})h\right], \qquad (22)$$

$$\Delta F_m = \frac{1-\gamma}{2}\left[\sigma_{xi,r}x^2 + \sigma_{yi,r}(x+\frac{h}{2})h\right].$$

These forces are then accumulated at each node: $F_k \leftarrow F_k + \Delta F_k$, $F_m \leftarrow F_m + \Delta F_m$.

7. DO 8, k = 1,...,N_k (all nodes).

8. Calculate $v_{k,r} = v_{k,r-1} + (F_k + f_e + f^{ext}_{k,r})\Delta t/(\rho h x^2)$ and $u_{k,r} = u_{k,r-1} + \Delta t\, v_{k,r}$.

For more detailed explanations, a similar algorithm for uniaxial stress wave given in Ref. 19 may be consulted. It may be checked that summing all the nodal forces (according to Eqs. 21-22) which act on one node yields a second-order discrete approximation of the continuum equation of motion, Eq. 18.

Figs. 7-8 show the numerical results obtained with the foregoing algorithm for the special case of volumetric strain-softening (28). The shear moduli G and $\bar{G}$ are assumed to be negligibly small (10^{-6}), and the bulk behavior follows the bilinear total stress-strain diagram in Fig. 9, characterized by elastic bulk moduli $\bar{K} = \bar{K}_0 = 1$, strain $\varepsilon_p = 1$ at

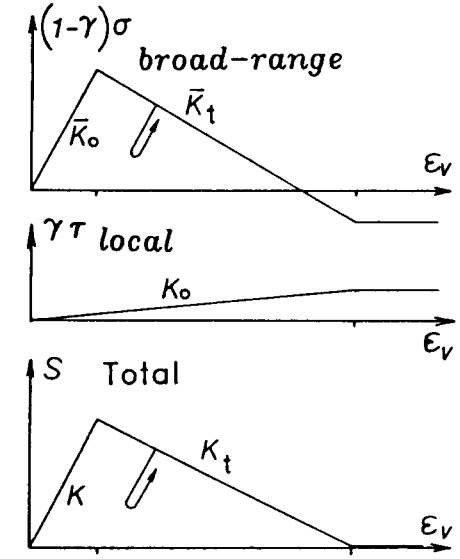

Figure 9. Local and nonlocal stress-strain relations assumed in examples

peak stress, and $\varepsilon_f = 5$ at the end of softening. This diagram is obtained by assuming that the local behavior is elastic-ideal plastic, and that the broad-range behavior (Fig. 9) exhibits oversoftening, the purpose of which is to achieve that, for the total behavior, the strain-softening terminates at exactly zero stress (19). The dimensions are $a = 10$, $b = 100$, $L = b - a = 90$. The use of coefficient γ is required for stability. For one-dimensional planar waves, it was shown (16) that stability is assured for $\gamma > 0$. However, γ-values too close to 0 are not possible for numerical solutions since they lead to an ill-conditioned equation system and produce excessive noise. For one-dimensional planar waves, the value $\gamma = 0.1$ gave noise-free response. The same value sufficed for the spherical wave ($\gamma = 0.1$), in order to obtain a response with noise-free appearance. The value of the applied surface pressure is chosen as $p_0 = 0.708$. For this boundary condition, the wave propagating from the outer surface remains elastic until the wavefront reaches 30% of the thickness $b - a$.

The nonlocal inelastic finite element program was first verified by running with it the solution for the special case of an elastic local material, for which one may set $\varepsilon_p = 10^8$, $\varepsilon_f = 10^9$, $\ell = h$ = mesh step (ℓ is variable here). The convergence with increasing numbers of elements (N =10, 20, 40, 80, 160) was good (28). The results for the spherical wave converge (quadratically) to the exact solution given by Eq. 19 (28). Subsequently, the problem was solved (28) for a nonlocal continuum ($\varepsilon_p = 1$, $\varepsilon_f = 5$) with the characteristic length $\ell = L/10 = 9$ = constant. The results for progressively refined meshes (N = 10, 20, 40, 80, 160) are shown in Figs. 7 and 8. For comparison, the solution was also run for a local continuum ($\ell = h = L/N$ = variable) having the same stress-strain relation with strain-softening.

The local and nonlocal results are compared in each figure. It is seen (Figs. 7-8) that the nonlocal solutions with strain-softening (right columns) converge well with increasing N. On the other hand, the corresponding local solutions (left columns) do not converge at all.

While an exact solution for a uniaxial planar wave in a local strain-softening material has previously been found (12) and the corresponding finite element solutions were shown to converge to it, for the present case no exact local solution with strain-softening has been found. The behavior of the local solutions is quite interesting. Similar to the exact solution for the planar wave, a strain-softening zone of finite size is apparently not obtained for the local material, and strain-softening appears to localize into singular points on the x-axis (the spikes in Figs. 7-8, left columns). These singular points begin to appear, as expected, when the strain at the wavefront grows to reach the strain-softening range, which cannot be closer than 0.3L from the outer surface, as already mentioned. However, in contrast to the planar wave, there is not only one singular point but many, and they appear at different locations for different N (i.e., different mesh refinements). The impression is that of chaos (reminiscent of the situation in turbulence). The reason for the appearance of a sequence of strain-softening points (the spikes in Figs. 7-8, left columns) is that part of the strain step at the wavefront is transmitted across the point of strain-softening before the stress is reduced to zero. This part of the wave which has crept through represents again an elastic strain wave with a step front, which then grows as the wavefront propagates further until the elastic limit ε_p is reached again. Then the situation repeats itself.

A similar strain-softening problem has also been solved for cylindrical waves (28). A static two-dimensional imbricate finite element analysis of a fracture specimen is reported in Ref. 47.

To sum up, the numerical results for the spherical waves (28), as well as the result for planar waves (19), show that the imbricate nonlocal continuum is a mathematically sound model for strain-softening.

COMPARISON WITH STRAIN-SOFTENING FRACTURE MODELS OF HILLERBORG, WILLAM AND OTHERS

Let us now turn attention again to the crack band model, which represents a special case of the imbricate nonlocal approach when the element size is not less than ℓ. The crack band model (5,9,16,18,24), for which the basic ideas of a fixed width of a strain-softening crack band were proposed in 1974 on the basis of stability analysis (4), has three independent material parameters: fracture energy G_f, tensile strength f_t', and crack band front width w_c. The value of the strain-softening modulus E_t then follows from Eq. 3. When a curved shape of the strain-softening segment of the diagram is used, E_t should be interpreted as the mean slope of this segment. The shape of the strain-softening segment must of course be specified, too.

Although the optimum fit of the entire data set was obtained when $w_c = 3d_a$ for concrete (24) and $w_c = 5d_a$ for rock, it was found that within the relatively broad range $d_a \le w_c \le 10d_a$ (where d_a = maximum size of aggregate or grain) the effect of w_c in the fits of fracture test data (localized cracking) is weak, and almost equally good fits of the test data can be obtained with various values of w_c within this range. Another reason for choosing the value of $w_c = 3d_a$ for concrete was the fact that the corresponding E_t value seems to represent well the mean slope of the descending branch for some direct tensile tests in which the specimen appeared to be in an approximately homogeneous state of strain.

Therefore, as far as the analysis of localized fracture is concerned, only two independent parameters of the crack band model, namely f_t' and G_f, are important, same as for the fictitious crack model of Hillerborg et al. (36,44,45) and the composite damage model of Willam, Sture et al. (53,54). Although these two models have not yet been systematically compared with the basic fracture test data from the literature, they should be capable of representing these data equally well as the crack band model since they are essentially equivalent to it. Each of them is also characterized by two independent material parameters G_f and f_t' to be found from fracture test data.

Hillerborg's model (36,44,45), which represents an adaptation to concrete of the formulations of Barrenblatt, Dugdale, Knauss, Kfouri, Rice and others for ductile fracture of metals (2,30,38,37), considers a line crack with a sharp tip and assumes a stress-displacement relation for this crack to be the basic material characteristic. If this relation is approximated as linear, the relative displacement across the line crack is $\delta = (\sigma - f_t')/C_f$ where C_f is the slope; $C_f < 0$. The fracture energy is then represented by the area under this strain-softening stress-displacement diagram, i.e., $G_f = -f_t'^2/2C_f$, from which $C_f =$

$-f_t'^2/2G_f$. Equating this expression for G_f to that according to the crack band model we have $G_f = -f_t'^2/2C_f = w_c(E^{-1} + E_t^{-1})f_t'^2/2$, from which we obtain the equivalence condition

$$\frac{1}{C_f} = -w_c\left(\frac{1}{E} - \frac{1}{E_t}\right). \tag{23}$$

The same relation may be obtained by application of Rice's J-integral, or by considering uniaxial stress and equating the stress displacement relations for both models for a bar element of length $L_e \geq w_c$. For the crack band model, segment w_c of the length L_e exhibits strain-softening, while the rest of the bar element undergoes elastic unloading, as may be concluded from stability analysis (4,5). For Hillerborg's model, only one line crack is allowed within the bar length L_e, according to stability conditions. Thus, the declining portion of the $\sigma - \delta$ relationship is described according to these two models as

$$\delta(\sigma) = w_c\left(\frac{f_t' - \sigma}{-E_t} + \frac{f_t'}{E}\right) + (L_e - w_c)\frac{\sigma}{E} = \frac{f_t' - \sigma}{-C_t} + L_e\frac{\sigma}{E} \tag{24}$$

($E_t < 0$, $C_t < 0$), and it may be checked that this equation is satisfied for any σ if Eq. 23 holds true.

The composite damage (or composite fracture) model of Willam, Sture et al. (53,54), which represents an adaptation of Pietruszczak and Mróz's model for strain-softening in shear (46), assumes a line crack (or a narrow cracking strip) to be embedded within the finite element and the additional strain due to cracking to be added to that due to elastic deformation of the element. For uniaxial stress in a finite element of length L_e in a bar, one obtains for this element the same stress-displacement relationship as Eq. 24, which again confirms the equivalence of this model.

We may thus conclude that the crack band model, the fictitious crack model of Hillerborg et al., and the composite damage (or composite fracture) model of Willam et al. are equivalent for uniaxial stress, except that continuum concept in the crack band model makes no sense for $L_e < w_c$; but neither of the other models can be applied for this case because the continuum description is no longer admissible if $L_e < w_c$. For problems with localized fracture and arbitrary geometry, these three models are not exactly equivalent, but they are nearly equivalent, with differences that are probably too small to be clearly detected from test results. This is because, according to St. Venant's principle, only the total additional relative displacement due to cracking at the fracture front matters for the energy release rate from the entire body.

It has been claimed (53,54) that the composite damage (composite fracture) model and the fictitious crack model differ from the crack band model by having only two rather than three independent material constants, G_f and f_t'. However, this claim is unjustified because w_c, the third independent constant in the crack band model, has almost no effect in fitting fracture test data, as already pointed out, and can be only determined if the softening modulus E_t is specified independently, which was done in Ref. 23 on the basis of direct tensile tests.

It has been also claimed that the composite damage model and the fictitious crack model permit the use of finite elements of any size, L_e,

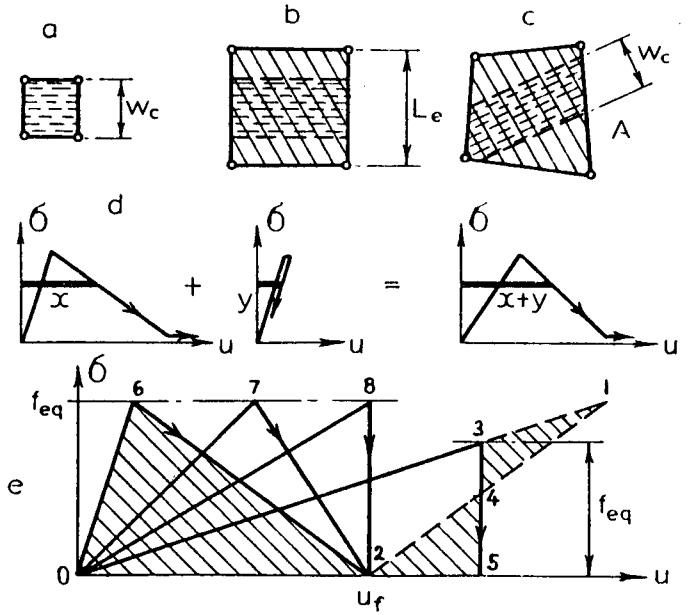

Figure 10. Crack band model when element size is increased (a–c), determination of overall stress-strain relation for finite element (d) and resulting stress-displacement relations for elements of various sizes

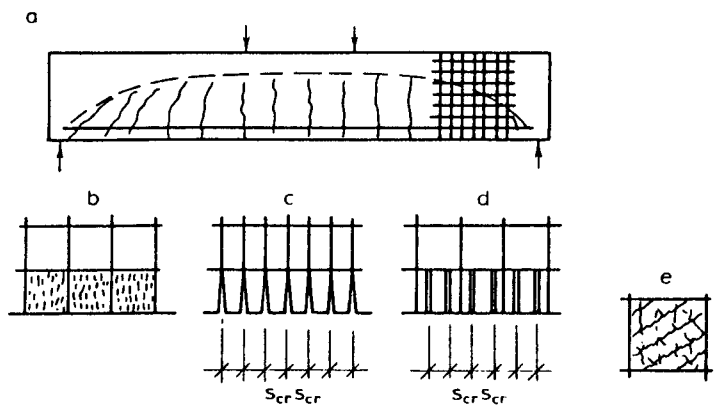

Figure 11. Nonlocalized distributed cracking (a,f) and its treatment by crack band model (b), fictitious crack model (c) and composite damage model (d)

whereas the crack band model is restricted to finite elements of size $L_e = w_c$. This is not true, however. As an approximation involving some error, the crack band model permits finite elements of sizes $L_e > w_c$ if the average stress-strain relation for the cracked finite element is modified (as shown in Refs. 9,16,17), and this modification turns out to yield the same stress displacement relation as the other two models. In general this modification may be formulated as follows.

Consider an arbitrary finite element of area A which has one integration point (and should not be too elongated in any direction); Fig. 10c. The overall stress-displacement relation for the entire element is obtained by adding the strain on the crack band of width w_c to the strain in the finite element (Fig. 10c). This yields for the mean strain tensor in the finite element the general rule

$$\underset{\sim}{\varepsilon} = \frac{w_c}{\sqrt{A}}\,\underset{\sim}{\varepsilon}_{soft} + \left(1 - \frac{w_c}{\sqrt{A}}\right)\underset{\sim}{\varepsilon}_{el} \tag{25}$$

where the element is approximately treated the same as a square element of side $\sqrt{A}$; $\underset{\sim}{\varepsilon}_{soft}$ is the strain according to the strain-softening constitutive relation for the crack band, and $\underset{\sim}{\varepsilon}_{el}$ is the elastic strain for the same stress value. It should be noted, though, that the use of an element size L_e that is too large may cause excessive numerical error.

Equation 25 assures that the energy dissipation at full cracking, as obtained from the stress-displacement relation for the entire element, is the same as the energy dissipation for the crack band w_c. This may be illustrated by the $\delta(\sigma)$ expression for uniaxial stress in Eq. 24. For various element lengths L_e, these relations give the curves in Fig. 10e. While the peak stress point in the stress-displacement relation moves to the right as the element length L_e increases, the end point with $\sigma = 0$ remains fixed because the area under this diagram, representing the fracture energy, must remain constant. The declining portion of the $\delta(\sigma)$ diagram has the inverse slope $d\delta/d\sigma = (w_c/E_t) + (L_e - w_c)/E$; it becomes steeper as L_e increases (Fig. 10e) and becomes vertical when $L_e = L_{cr}$,

$$L_{cr} = w_c\left(1 + \frac{E}{-E_t}\right) = \frac{2G_f E}{f_t'^2} \qquad \left(\frac{d\sigma}{d\delta} \to \infty\right). \tag{26}$$

For $L_e > L_{cr}$, the post-peak portion of the $\delta(\sigma)$ diagram has a positive slope. The post-peak states are then unstable under displacement control (the snap-back instability). This means that a static analysis of strain-softening problems becomes impossible. The response of the finite element system after the peak is *dynamic* and the inertia forces must be taken into account.

However, if only the final static state after strain-softening is of interest, strain-softening problems can be analyzed statically even for $L > L_{cr}$ provided that the post-peak response of positive slope is replaced by an equivalent vertical stress drop (Fig. 10e). This drop represents a dynamic motion which begins and ends with a zero kinetic energy. Consider the vertical stress drop $\overline{35}$ in Fig. 10e. The potential energy represented by area $\overline{134}$ accelerates the motion along segment $\overline{34}$, and the potential energy represented by area $\overline{245}$ decelerates the motion along segment $\overline{45}$. If these two potential energies cancel each other, i.e., if the areas $\overline{134}$ and $\overline{245}$ are the same, then the motion which begins

with an equilibrium state at point 3 will end with an equilibrium state (zero kinetic energy) at point 5. On the other hand, if the areas $\overline{134}$ and $\overline{245}$ were unequal, the final state at point 5 would not be an equilibrium state and a static analysis would then be incorrect.

We may conclude that, for the purpose of static analysis, in which some finite elements are larger than L_{cr}, the reverse post-peak behavior with positive slope can be replaced by a vertical stress drop for which the areas $\overline{134}$ and $\overline{245}$ in Fig. 3e are equal. This means that the area $\overline{035}$ under the entire diagram with the vertical stress drop must be equal to the area $\overline{012}$ under the actual stress-displacement diagram for the finite element of length L_e, which in turn equals the fracture energy G_f. Thus, the strength limit at the beginning of the equivalent vertical stress drop, which has been called the equivalent strength f'_{eq} (9,16,18), must satisfy the condition $f'_{eq}\,\delta_0/2 = G_f$ where $\delta_0 = L_e f'_{eq}/E$. This yields for the equivalent strength at $L_e > L_{cr}$ the expression

$$f'_{eq} = \sqrt{\frac{2G_f E}{L_e}} = f'_t\sqrt{w_c\left(1 - \frac{E}{E_t}\right)}\,\frac{1}{\sqrt{L_e}}\,. \tag{27}$$

This is the same expression as that deduced before in a different manner (9,16,18). We see that, for $L_e > L_{cr}$, the strength limit used in the calculation must be decreased in inverse proportion to $\sqrt{L_e}$.

When the vertical stress drop is used, and the mesh is not too crude, the results of analysis are very close to those of linear elastic fracture mechanics. The essential nonlinear characteristics of the response are caused by strain-softening, and so the strain-softening behavior cannot be analyzed with large elements that require a vertical stress drop, unless the structure is so large that linear elastic fracture analysis is applicable.

In the preceding we considered only the situations where the front of distributed cracking is known to localize to its minimum admissible width (w_c in the crack band model, zero in Hillerborg's and Willam's models). When typical fracture specimens are analyzed by finite elements, we know from testing experience that such complete localization will occur. Fracture test specimens are of course designed to obtain just that (localized fracture). In general situations, though, it is not known whether complete localization of the cracking front will occur, and in many practical situations it will not. For example, large, nonlocalized zones of distributed cracking may develop if they are stabilized by compression zones ahead of the cracking front, by reinforcement, or by boundary restraint (Fig. 11). Whether or not complete localization occurs must be decided on the basis of stability criteria, which are discussed in detail in Ref. 10.

The crack band model is ideally suited to handle also the situations of nonlocalized cracking. No additional material parameters are needed for this purpose because a stress-strain relation is used.

On the other hand, further extensions are needed for Hillerborg's fictitious crack model and Willam-Sture's composite damage model in order to handle nonlocalized cracking. An array of line cracks must be introduced for these models, either as a system of interelement line cracks or as a system of cracks with two or more cracks (or cracking strips) embedded in each finite element (see Fig. 10). These line

cracks cannot have arbitrary spacing s_{cr}, or else the analysis would be unobjective; any desired results could be obtained depending on the analyst's choice of s_{cr}. This is illustrated by the example in Fig. 12 which was solved at Northwestern University by P. Pfeiffer and is similar to an example presented before by Crisfield (29). The solution is given for a reinforced bar of length 10 in., concrete cross section A_c = 2 in.^{2}, steel cross section A_s = 0.1 in.^{2}, elastic moduli of steel and concrete $E_c = 4 \times 10^6$ psi, $E_s = 30 \times 10^6$ psi, and straight-line softening diagram of concrete with $E_t = -E_c/8$. The stress displacement relation is assumed so that it gives the same displacement over an element of length 2 in. (Eq. 23). It may be checked by stability criteria (4) that in this bar a uniformly distributed strain-softening is stable and no localization occurs. Three meshes of element sizes 4:2:1 are used, and the calculated load displacement diagrams (Fig. 12) are identical for the crack band model. However, for Hillerborg's and Willam's models, in which one line crack or crack strip per element (or per node) is implied, the results are very different (Fig. 12), illustrating that these models are for nonlocalized cracking unobjective with regard to the choice of element size.

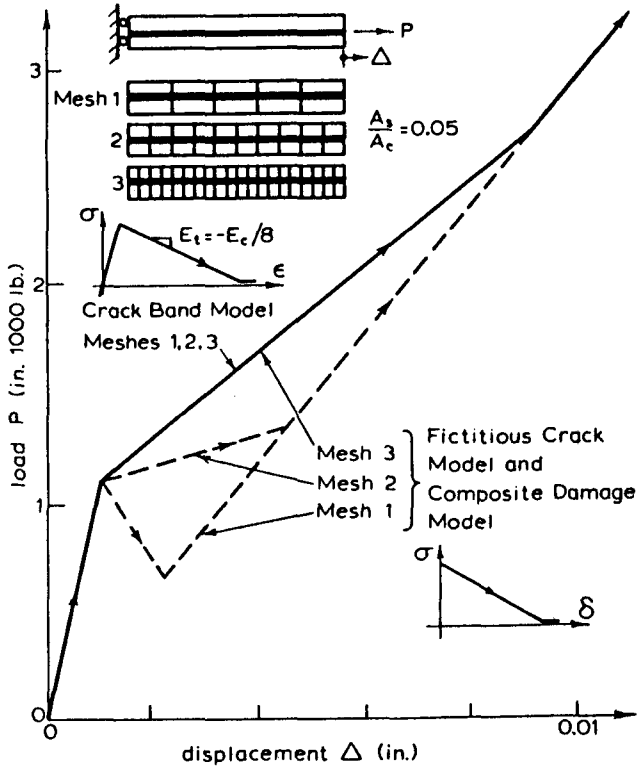

Figure 12. Finite element results of Pfeiffer and Bažant for three different meshes, for concrete bar with 5% reinforcement (nonlocalized cracking)

Thus we again see that the previous claims that these models with line cracks have one independent material parameter less than the crack band model (i.e., two vs. three) are unjustified. These models with line cracks require a characteristic length such as spacing s_{cr} as the *third* material parameter in order to be capable of handling any situations more general than the fracture specimens, which are designed so that the cracking is certain to localize.

It may be concluded that no strain-softening fracture model can be objective with regard to mesh size unless it involves some characteristic length as a material property. The situation is summarized in Table 1.

Table 1. Attainment of Objectivity with Respect to Element Size

Model	Localized Cracking	Nonlocalized Cracking
1. Classical Smeared Cracking	NO	YES
2. Fictitious Crack Model	YES	NO
3. Composite Damage Model	YES	NO
4. Crack Band Model	YES	YES

Aside from the foregoing limitation, Hillerborg's and Willam-Sture's models with line cracks do not seem very suitable for handling the situations where cracking orientation varies over the space (Fig. 11f). These models require proper crack spacing s_{cr} to be objective, but what is the proper spacing if the cracks are nonparallel? This must be expected in general situations. The question how to handle such situations apparently has not yet been addressed, and would have to be addressed if these models should be implemented in a general finite element code. A strain-softening constitutive relation appears to be the only practically manageable way to deal with nonlocalized cracking whose orientation is spatially variable (Fig. 11f).

Other behaviors which have been modeled with the crack band approach but appear difficult for the models based on line cracks are: 1) cracking in more than one direction at a point and 2) cracking process where the prevailing crack direction at one point changes its orientation during the loading process (for example, when partial cracks form in one direction, and later, after the principal stress has rotated, further cracks form in another direction).

CONSTITUTIVE RELATIONS FOR STRAIN-SOFTENING

In the analysis of many practical situations, including all fracture tests, the principal stress direction in the fracture process zone remains constant during fracturing. Triaxial strain-softening can then be introduced in the form of Eqs. 1 and 2. However, especially in dynamics, it is often necessary to describe progressive formation of fracture during which the principal stress directions rotate. In such a case, Eqs. 1-2 are inadequate. A satisfactory formulation can be obtained with an analog of the slip theory of plasticity (3,52), which has been called the microplane model (6,9,25). In this model it is assumed that the strain on a plane of any inclination consists of the resolved components of one and the same macroscopic strain tensor ε_{ij}. Using the

condition of equal energy dissipation when calculated in terms of the stresses and strains on all such planes and in terms of the macroscopic stress and strain tensors, one may obtain (6,9,25) the stress-strain relation

$$d\sigma_{ij} = D^c_{ijkm}\, d\epsilon_{ij} \tag{28}$$

in which

$$D^c_{ijkm} = \int_0^{2\pi} \int_0^{\pi/2} n_i n_j n_k n_m\, F'(e_n) \sin\phi\, d\theta d\phi. \tag{29}$$

This equation superimposes contributions to inelastic stress relaxations from the planes of all directions within the material, defined by spherical coordinates θ and ϕ; n_j are the direction cosines for all such directions, and $F(e_n)$ is a function characterizing the constitutive properties and representing the stress-strain relation for one particular microplane within the material; $e_n = n_i n_j \epsilon_{ij}$ = normal strain on a plane with direction cosines n_i. The integral in Eq. 24 must be evaluated numerically. Efficient numerical integration formulas for integration on the surface of a sphere are given by Stroud (48), and some further formulas which are superior in certain situations are given in Ref. 26. It has been demonstrated that the microplane model allows description of tensile strain-softening under general stress or strain histories and always leads to a reduction of stress to zero at sufficiently large tensile strain (26,9).

SIZE EFFECT LAW AND ITS GENERALIZATION

From the practical viewpoint, the imbricate nonlocal continuum model, as well as the special case of crack band model, differs from the usual local finite element models principally by the size effect. The structural size effect, a salient aspect of fracture mechanics, is observed when geometrically similar structures of different characteristic dimensions d are compared. It can be described in terms of the nominal stress at failure, defined as $\sigma_N = P/bd$ where P = load at failure (maximum load) and b = structure thickness. While according to the strength or yield criteria used in plastic limit design or elastic allowable stress design, σ_N is independent of structure size d, in fracture mechanics σ_N decreases as the structure size increases. This is because fracture mechanics is based on energy criteria for failure.

On the basis of an approximate but apparently quite reasonable hypothesis that the energy release caused by fracture is a function of both the fracture length and the area traversed by the fracture process zone, it can be shown (8) by dimensional analysis and similitude arguments that, for geometrically similar structures or specimens,

$$\sigma_N = Bf'_t\left(1 + \frac{d}{\lambda_0 d_a}\right)^{-\frac{1}{2}} \tag{30}$$

in which f'_t is the direct tensile strength of concrete, d_a is the maximum aggregate size, and d, λ_0 are empirical parameters characterizing the shape of the structure or specimen. According to this size effect law, the plot of log σ_N vs. log (d/d_a) represents a gradual transition from the strength criterion (i.e., σ_N proportional to strength f'_t) to the failure criterion of the classical, linear elastic fracture mechanics

(i.e., σ_N proportional to $d^{-\frac{1}{2}}$). This size effect law is verified, within the limits of inevitable statistical scatter, by all available Mode I fracture tests of concrete and mortar. The size effect law in Eq. 26 applies not only to cleavage (Mode I) fractures but also to shear (Mode II) fractures (27). Moreover, this size effect law has also been shown applicable to the diagonal shear failure of longitudinally reinforced beams without stirrups, unprestressed (23) or prestressed (13), punching shear of slabs (15), failure of unreinforced pipes (14), and is probably applicable to all the so-called brittle failures of reinforced concrete structures. Evaluation of fracture tests for different specimen sizes on the basis of Eq. 26 offers the simplest means for determining the fracture energy and other nonlinear fracture parameters.

When the usual, local finite element codes are applied to similar structures with similar meshes, the results exhibit no size effect. On the other hand, when the nonlocal model (or the special case of crack band model) is used, the results conform to the size effect law in Eq. 26, as experience confirms.

The size effect law in Eq. 30 was originally derived by dimensional analysis and similitude arguments from the following fundamental hypothesis:

The total potential energy release W caused by fracture in a given structure is a function of both

1. The length of the fracture a; and
2. The area of the cracked zone, $nd_a a$.

nd_a is a material constant representing the effective width of the microcracking zone at the fracture front, and d_a is the maximum aggregate size.

The original derivation (8), which used the nondimensional variables $\alpha_1 = a/d$ and $\alpha_2 = nd_a a/d^2$, tacitly implied one further hypothesis, namely that W as a function of the cracked zone area can be linearized. This is because otherwise the functions α_1 and α_2 used in Ref. (8) would not be size-independent as parameter α_2 depends on the relative size d_a/d when a/d is constant. This fact, as well as the need for the additional linearization assumption, was independently discovered by J. Planas and M. Elices (47).

We will now show a different derivation of the size effect law which involves linearization only as an asymptotic approximation that is always admissible, and which at the same time shows a more general form for the size effect law. Instead of the aforementioned nondimensional variables α_1 and α_2, we now choose as nondimensional variables:

$$\theta_1 = \frac{a}{d}, \quad \theta_2 = \frac{nd_a a}{ad} = \frac{nd_a}{d}. \tag{31}$$

We consider geometrically similar structures of different sizes d, which are characterized by a constant ratio a/d. Thus, parameter θ_1 is size-independent, while parameter θ_2 characterizes the size. As before (8), the potential energy release W of any structure may always be written in the form

$$W = \frac{1}{2E_c}\left(\frac{P}{bd}\right)^2 bd^2\, F(\theta_1, \theta_2, \epsilon_i) \tag{32}$$

in which E_c is the Young's elastic modulus of concrete, b is the thickness of the structure, P is the maximum load (i.e., the failure load in a load-controlled test), F is a certain function of nondimensional parameters, and ξ_1 are parameters characterizing the structure shape (geometry) which are constant when geometrically similar structures are considered. The nominal stress at failure may be defined as $\sigma_N = P/bd$. Then, substituting $P = \sigma_N bd$ and Eq. 32 into the well known fracture equilibrium relation

$$\frac{\partial W}{\partial a} = G_f b \tag{33}$$

where G_f is the fracture energy, we obtain

$$\frac{1}{2E_c}\frac{\sigma_N^2 b^2 d^2}{b}\frac{\partial F}{\partial \theta_1}\frac{1}{d} = G_b b \tag{34}$$

from which

$$\sigma_N = (2G_f E_c)^{\frac{1}{2}}\left[\frac{\partial F(\theta_1,\theta_2,\xi_1)}{\partial \theta_1}\, d\right]^{-\frac{1}{2}}. \tag{35}$$

In this formulation, the fracture energy itself is considered to be size-independent, being regarded as the final value of the R-curve. According to the blunt crack band theory, $G_f = nd_a(1 - E_c/E_t)f_t'^2/2E_c$, in which f_t' = direct tensile strength and E_t = mean slope of the strain-softening portion of the stress-strain diagram = strain-softening modulus. After substitution for G_f, Eq. 35 becomes

$$\sigma_N = \left[\frac{nd_a}{d}\left(1 - \frac{E_c}{E_t}\right)\right]^{\frac{1}{2}} f_t'\left[\frac{\partial F(\theta_1,\theta_2,\xi_1)}{\partial \theta_1}\right]^{-\frac{1}{2}}. \tag{36}$$

We may now choose the state $\theta_2 = 0$, which corresponds to an infinitely large structure, $d/d_a \to \infty$, as the reference state, and expand $\partial F/\partial\theta_1$ as a function of θ_2 in Taylor series. However, it is preferable to expand, more generally, the function $g(\eta) = (\partial F/\partial\theta_1)^r$ where $\eta = \theta_2^r$ and exponent r ($r > 0$) is an empirical constant to be chosen so that the size effect could be described with the minimum number of terms in the series expansion. Thus we may set

$$g(\eta) = \left[\frac{\partial F(\theta_1,\theta_2,\xi_1)}{\partial \theta_1}\right]^r = c_0 + c_1\eta + c_2\eta^2 + c_3\eta^3 + c_4\eta^4 + \cdots \tag{37}$$

in which

$$c_0 = \left[\left(\frac{\partial F}{\partial\theta_1}\right)^r\right]_{\theta_2=0}, \quad c_1 = \frac{1}{1!}\left[\frac{\partial}{\partial\eta}\left(\frac{\partial F}{\partial\theta_1}\right)^r\right]_{\theta_2=0},$$
$$c_2 = \frac{1}{2!}\left[\frac{\partial^2}{\partial\eta^2}\left(\frac{\partial F}{\partial\theta_1}\right)^r\right]_{\theta_2=0}, \quad c_3 = \frac{1}{3!}\left[\frac{\partial^2}{\partial\eta^2}\left(\frac{\partial F}{\partial\theta_1}\right)^r\right]_{\theta_2=0}, \cdots \tag{38}$$

Now, introducing $\partial F/\partial\theta_1 = [g(\eta)]^{1/r}$ into Eq. 36 and substituting Eq. 37 for $g(\eta)$, we can rearrange the resulting expression to the form

$$\sigma_N = Bf_t'\left[\left(\frac{\lambda_0}{\lambda}\right)^{-r} + 1 + \left(\frac{\lambda_1}{\lambda}\right)^r + \left(\frac{\lambda_2}{\lambda}\right)^{2r} + \left(\frac{\lambda_3}{\lambda}\right)^{3r} + \cdots\right]^{-1/2r} \tag{39}$$

in which $\lambda = d/d_a$ = relative size of the structure, and

$$B = c_1^{-1/2r}(1 - E_c/E_t)^{\frac{1}{2}}, \quad \lambda_0 = n(c_1/c_0)^{1/r},$$
$$\lambda_1 = n(c_2/c_1)^{1/r}, \quad \lambda_2 = n(c_3/c_1)^{1/2r}, \quad \lambda_3 = n(c_4/c_1)^{1/3r}, \ldots \tag{40}$$

Constants B, λ_0, λ_1, must normally be determined from maximum load data for geometrically similar specimens of different sizes. These constants are different for each specimen geometry. Note also that they are size-independent, since they depend on the derivatives of $F(\theta_1,\theta_2,\xi_1)$ at a fixed value of size parameter θ_2.

Eq. 39 is the most general asymptotic approximation for the size effect. However, full generality is preserved even if we substitute $r = 1$ because any smooth function $g(\eta)$ in Eq. 37 can be approximated by a polynomial with any desired degree of accuracy. The usefulness of coefficient r consists in the fact, found by experience, that if we use a certain optimal value of r we can describe any given shape of the size effect curve with much fewer terms than if we used $r = 1$. It is more effective to vary r than to include more terms in the series expansion.

If the structure is very large ($d/d_a \to \infty$), the first term in the brackets in Eq. 39 dominates over all other terms, which may be neglected. Then Eq. 39 reduces to

$$\sigma_N = Bf_t'(\lambda_0\, d_a/d)^{\frac{1}{2}} = \text{const.} \times d^{-\frac{1}{2}}. \tag{41}$$

This is the size effect typical of all solutions according to linear elastic fracture mechanics.

Eq. 41 represents the zero-th order asymptotic approximation of the size effect. The first-order approximation is obtained by retaining the first two terms of the series in Eq. 41 and truncating the rest:

$$\sigma_N = Bf_t'\left[1 + \left(\frac{d}{\lambda_0 d}\right)^r\right]^{-1/2r}. \tag{42}$$

This formula, which may be called the generalized size effect law since for $r = 1$ it reduces to the originally proposed approximate size effect law (Eq. 30), can closely represent various size effect curves which may be obtained by finite element analysis for various shapes of the softening diagram (11). It is hardly conceivable that an asymptotic approximation of higher than first order might be needed, provided that the optimum value of r for given data is used. However, if r were fixed as 1, then higher order approximations would be needed to closely describe certain finite element results for σ_N.

The size of the smallest castable concrete structure is a certain fixed multiple of the maximum aggregate size, say $d = 3d_a$. Substituting this into Eq. 42 or Eq. 39, we find that

$$\sigma_N = B_0 f_t' \tag{43}$$

in which B_0 is a constant for a particular geometry of the structure. Eq. 43 coincides with the failure criterion used in limit analysis (plasticity) as well as in the elastic allowable stress design. This criterion, as is well known, exhibits no size effect.

The size effect law in Eq. 30 or Eq. 42 offers the simplest means of determining the fracture parameters of concrete, particularly the frac-

15. Bažant, Z.P., and Cao, Z., "Size Effect in Punching Shear Failure of Slabs," Report No. 85-8/4285, Center for Concrete and Geomaterials, Northwestern University, Evanston, Illinois, May 1985.

16. Bažant, Z.P., Cedolin, L., "Blunt Crack Band Propagation in Finite Element Analysis," Journal of the Engineering Mechanics Division, ASCE, Vol. 105, No. EM2, April 1979, 207-315.

17. Bažant, Z.P., Cedolin, L., "Fracture Mechanics of Reinforced Concrete," Journal of the Engineering Mechanics Division, ASCE, Vol. 106, No. EM6, Dec. 1980, 1287-1306; with Discussion, Vol. 108, 1982, pp. 464-471.

18. Bažant, Z.P., Cedolin, L., "Finite Element Modeling of Crack Band Propagation," Journal of Structural Engineering, ASCE, Vol. 109, No. ST2, Feb. 1983, 69-92.

19. Bažant, Z.P., Chang, T.P., Belytschko, T.B., "Continuum Theory for Strain-Softening," Report No. 83-11/428c, Center for Concrete and Geomaterials, Northwestern University, Evanston, Ill., Nov. 1983; also Journ. Eng. Mech. ASCE, Vol. 111, Dec. 1984, 1666-1692.

20. Bažant, Z.P., and Chang, T.P., "Imbricate Finite Element Analysis of Strain-Softening Solids," Report No. 85-8/428, Center for Concrete and Geomaterials, Northwestern University, Evanston, Ill., Aug. 1985.

21. Bažant, Z.P., and Gambarova, R.G., "Crack Shear in Concrete: Crack Band Microplane Model," J. of Engineering Mechanics ASCE, Vol. 110, Sept. 1984, 2015-2035.

22. Bažant, Z.P., Kim, J.-K., and Pfeiffer, P., "Nonlinear Fracture Properties from Size Effect Tests," J. of Structural Eng., ASCE, in press.

23. Bažant, Z.P., and Kim, J.-K., "Size Effect in Shear Failure of Longitudinally Reinforced Beams," ACI Journal, Vol. 81, 1984, 456-468.

24. Bažant, Z.P., Oh, B.H., "Crack Band Theory for Fracture of Concrete," Materials and Structures (RILEM, Paris), Vol. 16, 1983, 155-177.

25. Bažant, Z.P., Oh, B.H., "Microplane Model for Fracture Analysis of Concrete Structures," Proc. Symp. on the Interaction of Nonnuclear Munitions with Structures, U.S. Air Force Academy, Colorado Springs, May, 1983, 49-55.

26. Bažant, Z.P., and Oh, B.H., "Microplane Model for Progressive Fracture of Concrete and Rock," J. of Engineering Mechanics ASCE, Vol. 111, 1985, pp. 559-582.

27. Bažant, Z. P., and Pfeiffer, P. D., "Tests of Shear Fracture and Strain-Softening in Concrete," Proc. 2nd Symp. on "The Interaction of Non-Nuclear Munitions with Structures," Panama City Beach, Florida, Apr. 1985, pp. 254-264; and further extension in Matériaux et Constructions (RILEM, Paris), in press.

28. Belytschko, T.B., Bažant, Z.P., Hyun, V.V., Chang, T.P., "Strain-Softening Materials and Finite Element Solutions," Computers and Structures, in press.

29. Crisfield, M.A., "Difficulties with Current Numerical Models for Reinforced Concrete and Some Tentative Solutions," Proc., Intern. Conf. on "Computer Aided Analysis and Design of Concrete Structures," held in Split, Yugoslavia, Sept. 1984, ed. by F. Damjanić, E. Hinton et al., publ. by Pineridge Press, Swansea, U.K., 331-358.

30. Dugdale, D.S., "Yielding of Steel Sheets Containing Slits," J. of Mech. Phys. Solids, Vol. 8, 1960, 100-108.

31. Eringen, A.C., Edelen, D.G.B., "On Nonlocal Elasticity," Int. J. Engng. Science, Vol. 10, 1972, 233-248.

32. Eringen, A.C., Ari, N., "Nonlocal Stress Field at Griffith Crack," Cryst. Latt. Def. and Amorph. Mat., Vol. 10, 1983, 33-38.

33. Evans, R.H., Marathe, M.S., "Microcracking and Stress-Strain Curves for Concrete in Tension," Materials and Structures (RILEM, Paris), No. 1, Jan.-Feb., 1968, 61-64.

34. "Finite Element Analysis of Reinforced Concrete," ASCE State-of-the-Art Report prepared by a Task Committee chaired by A. Nilson, ASCE, New York, 1982.

35. Heilmann, H.G., Hildsdorf, H.K., Finsterwalder, K., "Festigkeit und Verformung von Beton unter Zugspannungen," Deutscher Ausschuss für Stahlbeton, Heft 203, W. Ernst & Sohn, West Berlin, 1969.

36. Hillerborg, A., Modéer, M., Petersson, P.E., "Analysis of Crack Formation and Crack Growth in Concrete by Means of Fracture Mechanics and Finite Elements," Cement & Concrete Research, Vol. 6, 1976, 773-782.

37. Kfouri, A.P., and Rice, J.R., "Elastic-Plastic Separation Energy Rate for Crack Advance in Finite Growth Steps," in Fracture 1977 (Proc. of 4th Intern. Conf. on Fracture, Waterloo, Ontario, June 1977), ed. by D.M.R. Taplin, Univ. of Waterloo Press, 1977, Vol. 1, 43-59.

38. Knauss, W.C., "On the Steady Propagation of a Crack in a Viscoelastic Plastic Solid," J. of App. Mech., ASME, Vol. 41, No. 1, 1974, 234-248.

39. Krŏner, E., "Elasticity Theory of Materials with Long-Range Cohesive Forces," Int. J. Solids Structures, Vol. 3, 1967, 731-742.

40. Krŏner, E., "Interrelations between Various Branches of Continuum Mechanics," Mechanics of Generalized Continua, ed. by E. Krŏner, Springer-Verlag, 1968, 330-340.

41. Krumhansl, J.A., "Some Considerations of the Relation between Solid State Physics and Generalized Continuum Mechanics," Mechanics of Generalized Continua, ed. by E. Krŏner, Springer-Verlag, 1968, 298-331.

42. Kunin, I.A., "The Theory of Elastic Media with Microstructure and the Theory of Dislocations," Mechanics of Generalized Continua, ed. by E. Krŏner, Springer-Verlag, 1968, 321-328.

43. Levin, V.M., "The Relation between Mathematical Expectation of Stress and Strain Tensors in Elastic Microheterogeneous Media," Prikladnaya Mathematika i Mekhanika, Vol. 35, 1971, 694-701 (in Russian).

44. Petersson, E., "Fracture Energy of Concrete: Method of Determination," Cement & Concrete Research, Vol. 10, 1980, 78-89, and Fracture Energy of Concrete, Practical Performance and Experimental Results," Cement and Concrete Research, Vol. 10, 1980, 91-101.

45. Petersson, P.C., "Crack Growth and Development of Fracture Zones in

Plain Concrete and Similar Materials," Doctoral Dissertation, Lund Institute of Technology, Lund, Sweden, Dec. 1981.

46. Pietruszczak, S., Mróz, Z., "Finite Element Analysis of Deformation of Strain-Softening Materials," Intern. J. of Num. Meth. in Engng., Vol. 17, 1981, 327-334.

47. Planas, J., and Elices, M., Private Communication to Z.P. Bažant, Dept. of Material Science, ETS Universidad Politecnica de Madrid, Spain, March 1985.

48. Stroud, A.H., Approximate Calculation of Multiple Integrals, Prentice Hall, Englewood Cliffs 1971, 296-302.

49. Rashid, Y.R., "Analysis of Prestressed Concrete Pressure Vessels," Nuclear Engng. & Design, Vol. 7, No. 4, April 1968, 334-344.

50. Reinhardt, H.W., Cornelissen, E., "Post-Peak Cyclic Behavior of Concrete in Uniaxial Tension and Alternating Tensile and Compressive Loading," Cement & Concrete Research, Vol. 14, 1984, 263-270.

51. Rüsch, H., Hilsdorf, H., "Deformation Characteristics of Concrete under Axial Tension," Vorunterschungen, Bericht Nr. 44, Munich, May 1963.

52. Taylor, G.I., "Plastic Strain in Metals," Jour. of the Institution of Metals (London), Vol. 62, 1938, 307-324.

53. Willam, K.J., Bicanić, N., Sture, S., "Constitutive and Computational Aspects of Strain-Softening and Localization in Solids," Proc. Sym. on Constitutive Equations, Micro, Macro & Computational Aspects, K.J. Willam, ed., held at ASME Winter Annual Meeting, New Orleans, Dec. 1984, Am. Soc. of Mech. Engrs., New York, 1984.

54. Willam, K.J., Hurlbut, B., Sture, S., "Experimental, Constitutive and Computational Aspects of Concrete Failure," Preprints, U.S.-Japan Seminar on Finite Element Analysis of Reinforced Concretes, Tokyo, May 1985, 149-172.

55. Wittmann, F.H. (editor), Fracture Mechanics of Concrete, Elsevier, Netherlands, 1983.